

## Morphotropic Phase Boundary in Polarized Organic Piezoelectric Materials

Fangfang Gao<sup>1,2,\*</sup>, Xuan Zhao<sup>1,2,\*</sup>, Xiaochen Xun<sup>1,2,\*</sup>, Houbing Huang<sup>3</sup>, Xiaoming Shi<sup>3</sup>, Qi Li<sup>1,2</sup>, Fang Liu<sup>4</sup>,  
Peng Gao<sup>4</sup>, Qingliang Liao<sup>1,2,†</sup> and Yue Zhang<sup>1,2,‡</sup>

<sup>1</sup>Academy for Advanced Interdisciplinary Science and Technology, Beijing Advanced Innovation Center for Materials Genome Engineering, University of Science and Technology Beijing, Beijing 100083, People's Republic of China

<sup>2</sup>Beijing Key Laboratory for Advanced Energy Materials and Technologies, School of Materials Science and Engineering, University of Science and Technology Beijing, Beijing 100083, People's Republic of China

<sup>3</sup>Advanced Research Institute of Multidisciplinary Science, Beijing Institute of Technology, Beijing 100081, China

<sup>4</sup>Electron Microscopy Laboratory and International Center for Quantum Materials, School of Physics, Peking University, Beijing 100871, China

 (Received 8 December 2022; accepted 17 May 2023; published 13 June 2023)

Designing the morphotropic phase boundary (MPB) has been the most sought-after approach to achieve high piezoelectric performance of piezoelectric materials. However, MPB has not yet been found in the polarized organic piezoelectric materials. Here, we discover MPB with biphasic competition of  $\beta$  and 3/1-helical phases in the polarized piezoelectric polymer alloys (PVTC-PVT) and demonstrate a mechanism to induce MPB using the compositionally tailored intermolecular interaction. Consequently, PVTC-PVT exhibits a giant quasistatic piezoelectric coefficient of  $>32$  pC/N while maintaining a low Young's modulus of 182 MPa, with a record-high figure of merit of piezoelectricity modulus of about 176 pC/(N · GPa) among all piezoelectric materials.

DOI: 10.1103/PhysRevLett.130.246801

The piezoelectrics, acting as indispensable materials in electromechanical systems, have been used in ultrasonic imaging devices [1], various wearable sensors [2], and underwater sonars [3]. To meet the increasing demands of advanced piezoelectric devices, especially high-resolution ultrasonic imagers and implantable ultrasensitive sensors, it is urgently necessary to obtain high piezoelectric performance [4,5]. Designing the morphotropic phase boundary (MPB) with biphasic competition has become the most effective approach to enhance piezoelectric performance [6,7] due to the ease of polarization rotation at the external electric field or stress [8,9]. But this physical concept has been exclusive to inorganic piezoelectric materials for the past few decades [10], ranging from Pb-based piezoelectrics like  $\text{Pb}(\text{Zr}_x, \text{Ti}_{1-x})\text{O}_3$ ,  $\text{Pb}(\text{Mg}_{1/3}\text{Nb}_{2/3})\text{O}_3$ - $\text{PbTiO}_3$  to Pb-free piezoelectrics like  $\text{Ba}(\text{Zr}, \text{Ti})\text{O}_3$ - $(\text{Ba}, \text{Ca})\text{TiO}_3$  and  $\text{Bi}_{1/2}\text{Na}_{1/2}\text{TiO}_3$ - $\text{BaTiO}_3$ .

MPB was only reported in a unpolarized piezoelectric copolymer in 2018 [11], in which the compositionally tailored tacticity induces the evolution from nonpolar phase to polar phases, contributing to biphasic competition between the  $\beta$  and 3/1-helical phases. But MPB has not yet been found in the polarized organic piezoelectric materials; i.e., because these organic materials are usually polarized by external electric fields to exhibit piezoelectricity. Their molecular conformations are easy to change at the poling field [12] and two phases are directly transformed into a single phase [13], resulting in the disappearance of the phase boundary. So far, there exists no

mechanism to induce MPB in polarized organic piezoelectric materials. These dilemmas hamper the piezoelectric performance improvement (quasistatic piezoelectric coefficient  $d_{33} < \text{about } 25$  pC/N [14,15]) and restrict the extensive applications of organic piezoelectric materials in wearables and bioelectronics [16].

In this Letter, we first achieve MPB in polarized piezoelectric polymer alloys (PVTC-PVT) with phase competition between  $\beta$  (all-trans  $T_{m>4}$ ; T, trans) and 3/1-helical ((TG)<sub>3</sub>/(TG')<sub>3</sub>; G, gauche) phases, which is induced by the compositionally tailored intermolecular interaction. With MPB, PVTC-PVT presents a giant piezoelectric coefficient while low modulus can be maintained. Its  $d_{33}$  is comparable to that of the best known single crystalline of P(VDF-TrFE), but the Young's modulus is 2.8% of the single crystalline modulus. The Young's modulus of PVTC-PVT reaches to the lowest value among the excellent-property piezoelectric materials.

The piezoelectric polymer alloy is designed by the miscibility of poly(vinylidene fluoride-trifluoroethylene-chlorofluoroethylene) [P(VDF-TrFE-CFE)] and poly(vinylidene fluoride-trifluoroethylene) [P(VDF-TrFE)] at a molecular level (The preparation and characterization are shown in Supplemental Material S1 [17]), which is demonstrated in Supplemental Material S2 [17]. To investigate the piezoelectric properties of PVTC-PVT, the PVTC-PVT with various components was fully polarized by the external electric field. The crystal structures of polarized PVTC-PVT at room temperature are displayed in Fig. 1(a).

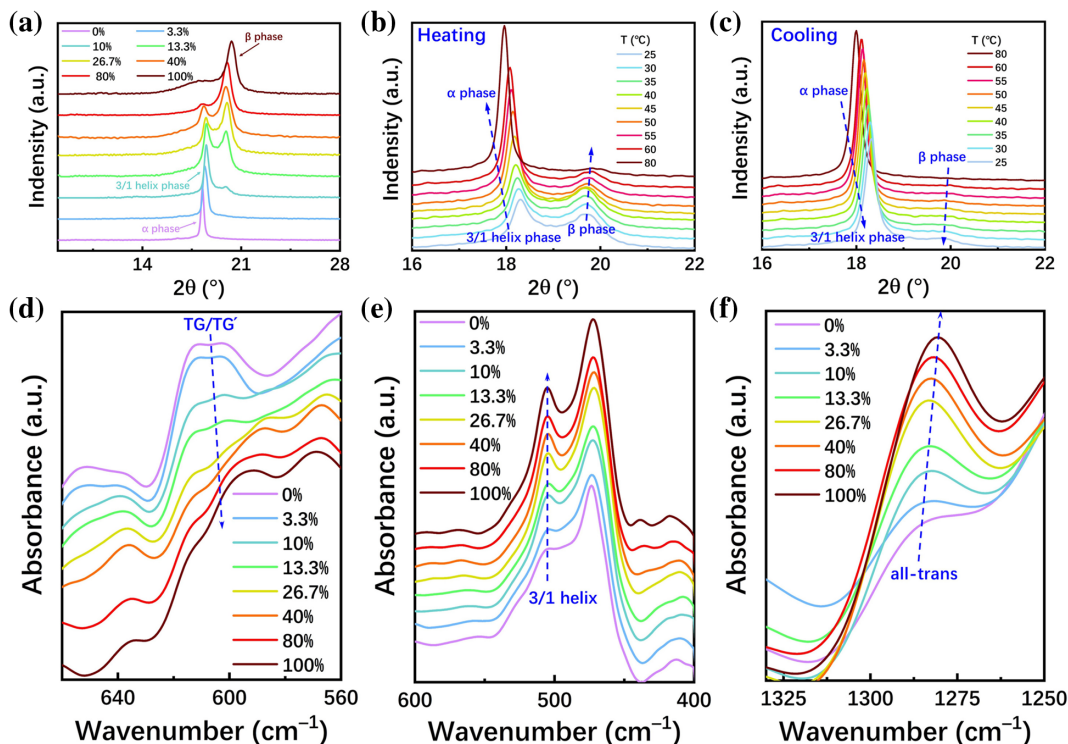


FIG. 1. (a) Crystal structure evolution of polarized PVTC-PVT with various compositions. (b) and (c) *In situ* XRD patterns of polarized PVTC-PVT at various temperatures. (d), (e), and (f) Infrared absorbance bands of polarized PVTC-PVT at around 610, 505, and 1280  $\text{cm}^{-1}$ .

The  $\alpha$  phase (TG/TG') of P(VDF-TrFE-CFE) gradually disappeared and is converted into the 3/1-helical phase and  $\beta$  phase with the P(VDF-TrFE) composition increasing, which is consistent with the FTIR results of Figs. 1(d)–1(f). Surprisingly, an obvious competition region between the  $\beta$  phase and 3/1-helical phase is found in PVTC-PVT with P(VDF-TrFE) content variation from 13.3 to 40 wt%, in according with the structural features of the MPB. To exclude the possibility of simple mixing of two phases, *in situ* XRD of polarized PVTC-PVT (80/20 wt%) at various temperatures is performed. As the temperature increases from 25  $^{\circ}\text{C}$  to 80  $^{\circ}\text{C}$  [Fig. 1(b)], the depolarization and Curie transition occurs. The  $\beta$  phase is transformed into 3/1-helical phase and then both  $\beta$  phase and 3/1-helical phase gradually disappeared. For the cooling process of Fig. 1(c), the  $\alpha$  phase is reversibly converted into the 3/1-helical phase and  $\beta$  phase. Not surprisingly, the  $\beta$  phase does not recover to a content before heating. Because part of the  $\beta$  phase in polarized PVTC-PVT is transformed from the 3/1-helical phase caused by the poling field, this transition cannot be carried out spontaneously without the poling field after the depolarization. The electric field-induced phase transition can be confirmed by the crystal structure difference before and after polarization [Fig. S1a in [17] and Fig. 1(a)]. These results sufficiently demonstrate that the 3/1-helical phase and  $\beta$  phase can transform each other, but not a simple two-phase mixture. The MPB is

possibly achieved in PVTC-PVT. The coexistence of the 3/1-helical phase and  $\beta$  phase can be confirmed in the FTIR experiments of Figs. 1(e) and 1(f). The absorbance band change of polarized PVTC-PVT is similar to that of the unpolarized PVTC-PVT.

To further demonstrate the existence of MPB, the physical and mechanical properties of PVTC-PVT are studied.  $d_{33}$  of polarized PVTC-PVT are measured by a quasistatic piezoelectric tester. As shown in Fig. 2(a), the quasistatic  $d_{33}$  first increases and then decreases. A maximum  $d_{33}$  of about 32 pC/N is obtained in the PVTC-PVT (73.3/26.7 wt%) at room temperature, which supports the performance characteristic caused by MPB [7,9].  $d_{33}$  calculated by the phase field simulation (Supplemental Material S1 [17]) is consistent with the experimental results, which verify the phase transition is responsible for the  $d_{33}$  change. Figure 2(b) indicates the Young's modulus of PVTC-PVT gradually ascends in general as a result of the increase of P(VDF-TrFE) with the higher modulus, where the Young's modulus is calculated by the corresponding stress-strain curve (Fig. S5 [17]) The PVTC-PVT (73.3/26.7 wt%) has a low Young's modulus of about 182 MPa. Generally speaking, the organic materials inevitably increase Young's modulus (>about 1 GPa) as they gain piezoelectric property. Here, the compatibility of two conflicting properties of high piezoelectric coefficient (>32 pC/N) and low Young's modulus (182 MPa) in

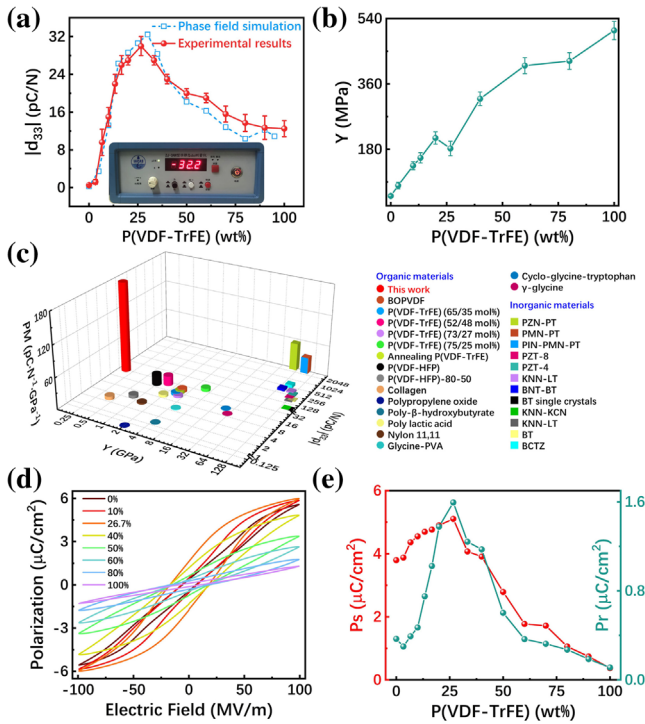


FIG. 2. (a)  $d_{33}$ , simulated  $d_{33}$  and (b) Young's modulus as a function of P(VDF-TrFE) contents, inset is a quasistatic piezoelectric tester. (c) Summary of  $d_{33}$ , Young's modulus, and figure of merit of piezoelectricity modulus for bulk piezoelectric materials reported in the literatures. (d) Polarization-electric field hysteresis loops of PVTC-PVT at a frequency of 5 Hz. (e) The  $P_s$  and  $P_r$  of PVTC-PVT versus different P(VDF-TrFE) contents.

organic materials is achieved for the first time. The  $d_{33}$  of PVTC-PVT is compared to that of the reported single crystalline of P(VDF-TrFE) (75/25 mol%), but our Young's modulus is 2.8% of its modulus [18]. Beyond that, the figure of merit of piezoelectricity modulus ( $PM = |d_{33}|/Y$ ) for different piezoelectric materials is calculated in Fig. 2(c). The PVTC-PVT exhibits an ultra-high PM of about 176 pC/(N·GPa) among all piezoelectric materials, which is 229% increasing over the state-of-the-art piezoelectric materials [15,16,18–27]. The low Young's modulus endows PVTC-PVT with exceptional biomechanicals compatible with human tissue. PVTC-PVT with high piezoelectricity meets the requirement of matching with the modulus of human tissue [28] (< about 480 MPa) to ensure long-term biointegration and minimize foreign-body reaction [29–31], which opens up new applicable scenarios for them in the wearables and bioelectronics. The temperature-dependent dielectric spectroscopies of PVTC-PVT at 100 kHz are displayed in Figs. S6(a) and S6(b). On the whole, the maximum dielectric constants ( $\epsilon_m$ ) of polarized PVTC-PVT first decreases and then increases, governed successively by the terpolymer and copolymer contents.  $\epsilon_m$  exhibits the abnormal properties at P(VDF-TrFE) of 3.3 and 26.7 wt %,

respectively. The abnormal improvement of  $\epsilon_m$  may be attributed to the interfacial couplings between terpolymer and copolymer crystallites at low component [32] and the MPB behavior at high component. The temperature dependence of dielectric spectroscopies for polarized PVTC-PVT at different compositions are shown in Fig. S6(c) [17]. The dielectric spectroscopies of polarized PVTC-PVT (P(VDF-TrFE) = 26.7 wt%) exhibit apparent frequency dispersion and diffuse phase transition. Moreover, the frequency dependence of the temperature ( $T_m$ ) at the dielectric peak is well fitted with Vogel-Folcher law [inset of Fig. S6(c) [17]]. These results fully demonstrate the polarized PVTC-PVT is of the relaxor ferroelectric properties [33]. So far, the macroscopical MPB for organic materials only was found in the relaxor ferroelectrics, not normal ferroelectrics, which is obviously different from the inorganic ferroelectrics [10]. Figure 2(c) reveals the dependence of composition on the polarization hysteresis loop. The polarization level of PVTC-PVT becomes increased and then decreased. The spontaneous polarization ( $P_s$ ) and remnant polarization ( $P_r$ ) are obtained by the Fig. 2(c).  $P_s$  and  $P_r$  as a function of P(VDF-TrFE) contents are shown in Fig. 2(d) and manifest the same trend as  $d_{33}$  change. A maximum  $P_s$  and  $P_r$  can reach to 5.1 and 1.6  $\mu\text{C}/\text{cm}^2$ , respectively. These behaviors sufficiently demonstrate the existence of MPB in PVTC-PVT.

With an increase of P(VDF-TrFE) content, the nonpolar  $\alpha$  phase of polarized PVTC-PVT is transformed into polar  $\beta$  and 3/1-helical phases, which induces the formation of MPB. The inducement mechanism of MPB is analyzed. From the results above (Supplemental Material S2 [17]), the intermolecular interaction between P(VDF-TrFE) and P(VDF-TrFE-CFE) reduces mixing  $\Delta G_m$  and leads to their miscibility at the molecular level. It is speculated that the phase transition of polarized PVTC-PVT is driven by the intermolecular interaction. To demonstrate this speculation, *in situ* temperature-dependent phase transition of polarized PVTC-PVT is first carried out. According to *in situ* temperature-dependent FTIR spectra in Figs. 3(a), 3(b) and S7(a) [17], the both 3/1-helical and all-trans conformation content of polarized PVTC-PVT gradually decreases and are converted into the TG/TG' conformation at the heating process. For the cooling process in Figs. S7(b)–S7(d), the TG/TG' conformation is reversibly converted into the 3/1-helical and all-trans conformation, but the all-trans conformation does not recover to the content before heating. Interestingly, the previous results indicate the 3/1-helical conformation is hardly affected by the temperature [11], because its chain structure resembles that of a disordered paraelectric phase. The similar case is also found in polarized PVTC-PVT with P(VDF-TrFE) content up to 80 wt % [Figs. S7(e) and S7(f) [17]]. The 3/1-helical conformation of PVTC-PVT is transformed from TG/TG' conformation at the low P(VDF-TrFE) content, which may

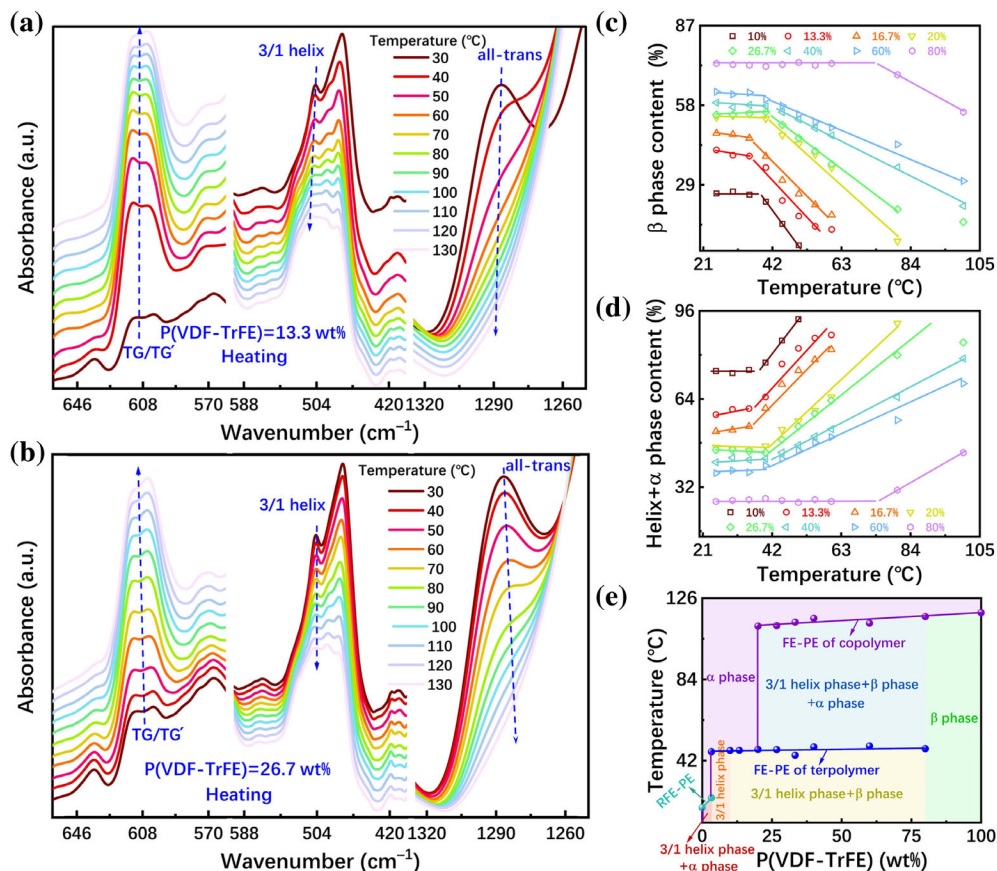


FIG. 3. (a) and (b) *In situ* temperature-dependent FTIR spectra of polarized PVTC-PVT at around 610, 505, and 1280  $\text{cm}^{-1}$ . (c) and (d) The  $\beta$  phase and 3/1-helical +  $\alpha$  phase contents as a function of the temperature. (e) Phase diagram of polarized PVTC-PVT.

be driven by the intermolecular interaction. Its temperature stability is closely related to the intermolecular interaction. The intermolecular interaction is easily destroyed at high temperature [34], due to the thermal motion of molecules, which results in a temperature-unstable 3/1-helical conformation. Once P(VDF-TrFE) exceeds a certain amount, the 3/1-helical conformation in polarized PVTC-PVT directly comes from P(VDF-TrFE) and can maintain stable at the high temperature.

Then, *in situ* XRD of polarized PVTC-PVT at various temperatures is studied and the different phase content can be calculated by the integral area of diffraction peaks [Figs. 3(c) and 3(d)]. As the temperature increases, the phase transition from ferroelectrics to paraelectrics occurs. The  $\beta$  phase content markedly decreases and the 3/1-helical +  $\alpha$  phase content have opposite trends. With P(VDF-TrFE) content increasing, the temperature stability of  $\beta$  phase in polarized PVTC-PVT is improved. The  $\beta$  phase with relatively low transition temperature is transformed from the  $\alpha$  phase of P(VDF-TrFE-CFE) through the intermolecular interaction. Once the P(VDF-TrFE) exceeds a certain amount, the part of  $\beta$  phase of polarized PVTC-PVT is directly derived from P(VDF-TrFE) with a high Curie temperature and  $\beta$  phase shows a high transition

temperature. The existence of two Curie temperatures in Fig. S8 [17] can prove this point. Besides, with the addition of P(VDF-TrFE) content to 80 wt %, the  $\beta$  phase content in polarized PVTC-PVT gradually increases and  $d_{33}$  presents obviously different change. Such a behavior confirms that the improvement of piezoelectric performance results from the MPB, not the  $\beta$  phase content, which is different from the previous report [15]. These results indicate that the intermolecular interaction drives the transition from the nonpolar phase to polar phases in PVTC-PVT. According to DSC and XRD of polarized PVTC-PVT [Fig. S8 [17] and Fig. 1(a)], the phase diagram about the transition temperature versus the P(VDF-TrFE) contents is drawn, as displayed in Fig. 3(c). There are three phase transitions in the phase diagram. Corresponding transitions are attributed to the Curie transition from the relaxor ferroelectric phase (RFE) of P(VDF-TrFE-CFE) to paraelectric phase (PE) below 22.8 °C during P(VDF-TrFE) range of 0 ~ 3.3 wt%, FE of P(VDF-TrFE-CFE) to PE at about 50 °C during the range of 3.3 ~ 80 wt% and FE of P(VDF-TrFE) to PE at about 116 °C during the range of 20 ~ 100 wt%, respectively. The research of phase transition clearly states that PVTC-PVT have rich and controllable phase structures, which not only gives the organic

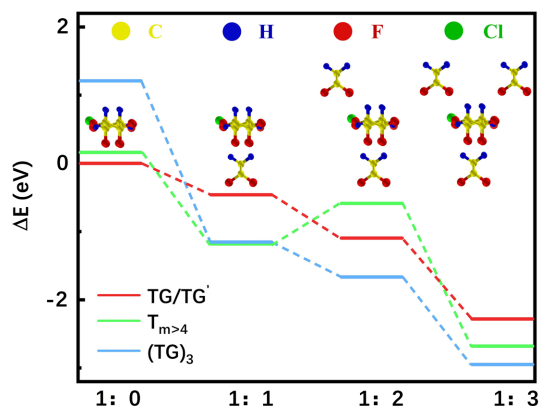


FIG. 4. Relative energy diagrams of P(VDF-TrFE-CFE) conformations.

materials exceptional physical and mechanical properties but provides an effective method for tailoring their properties.

Finally, the first-principles calculation using density functional theory (Supplemental Material S1 [17]) is adopted to verify further the speculation above. The relative energy diagrams ( $\Delta E = E_{\text{ter-chain}} - E_{\text{ground state}}$ ) of single molecular chain of P(VDF-TrFE-CFE) at the different P(VDF-TrFE) content is calculated by DFT, as shown in Fig. 4 and Fig. S9–S11. Here, the different single chain energy ( $E_{\text{ter-chain}}$ ) of P(VDF-TrFE-CFE) is defined as [35]

$$E_{\text{ter-chain}} = E_{\text{total}} - N \times E_{\text{cop-chain}},$$

where  $E_{\text{total}}$  is the total energy of a chain ( $T_{m>4}$ ,  $(TG)_3$  or  $TG/TG'$ ) of P(VDF-TrFE-CFE) and  $N$   $T_{m>4}$  chains of P(VDF-TrFE).  $E_{\text{cop-chain}}$ ,  $N$  are the energy and the number of  $T_{m>4}$  chain of P(VDF-TrFE), respectively. A  $TG/TG'$  chain of P(VDF-TrFE-CFE) is regarded as the ground state. When  $N = 0$ ,  $TG/TG'$  chain is lower in energy than  $T_{m>4}$  chain by 0.16 eV and  $(TG)_3$  chain by 1.21 eV, which results in P(VDF-TrFE-CFE) presents experimentally the  $\alpha$  phase ( $TG/TG'$  conformation). When  $N = 1$ , the energy of  $TG/TG'$ ,  $T_{m>4}$ , and  $(TG)_3$  in P(VDF-TrFE-CFE) are  $-0.46$ ,  $-1.18$ , and  $-1.15$  eV, respectively. The energy of polar  $T_{m>4}$  and  $(TG)_3$  are close, but lower than  $TG/TG'$  chain. As P(VDF-TrFE) continues to be added, the energy of polar phases of P(VDF-TrFE-CFE) is reduced and the polar phases are more stable, which are consistent with the experimental data. Arguably, the intermolecular interaction results in the transition of nonpolar phase into polar phases of PVTC-PVT (Table S1 [17]). Therefore, MPB is induced by the compositionally tailored intermolecular interaction. It follows that the inducement mechanism of PVTC-PVT is apparently different from that reported for P(VDF-TrFE) (49/51 mol%) [11].

In summary, we report a new mechanism to induce a MPB using the compositionally tailored intermolecular interaction. The intermolecular interaction drives the

transition from nonpolar phase to polar phases and induces the formation of MPB. A challenge that MPB is difficultly formed in polarized organic materials is overcome. As a result, the compatibility of high piezoelectricity and low modulus in PVTC-PVT is achieved. PVTC-PVT shows a highest figure of merit of piezoelectricity modulus, which is far superior to the state-of-the-art organic piezoelectric materials. This Letter provides a promising path to tailor phase structures and design high-performance organic piezoelectric materials from the molecular level. In addition, the discovery of MPB in a piezoelectric polymer alloy brings an opportunity to enrich the soft condensed matter physics and construct advanced wearable or bioelectronic devices.

This work was supported by the National Key Research and Development Program of China (No. 2018YFA0703500), the National Natural Science Foundation of China (No. 52232006, No. 52188101, No. 52102153, No. 52072029, No. 51991340, and No. 51991342), the Overseas Expertise Introduction Projects for Discipline Innovation (B14003), the China Postdoctoral Science Foundation (2021M700379) and the Fundamental Research Funds for Central Universities (FRF-TP-18-001C1).

\*These authors contributed equally to this work.

†Corresponding author.

liao@ustb.edu.cn

‡Corresponding author.

yuezhang@ustb.edu.cn

- [1] L. V. Wang, *Nat. Photonics* **3**, 503 (2009).
- [2] W. Yan *et al.*, *Nature (London)* **603**, 616 (2022).
- [3] Q. M. Zhang, V. V. Bharti, and X. Zhao, *Science* **280**, 2101 (1998).
- [4] F. Li *et al.*, *Science* **364**, 264 (2019).
- [5] C. Dagdeviren *et al.*, *Proc. Natl. Acad. Sci. U.S.A.* **111**, 1927 (2014).
- [6] R. J. Zeches *et al.*, *Science* **326**, 977 (2009).
- [7] C. Ma, H. Guo, S. P. Beckman, and X. Tan, *Phys. Rev. Lett.* **109**, 107602 (2012).
- [8] H. Fu and R. E. Cohen, *Nature (London)* **403**, 281 (2000).
- [9] W. Liu and X. Ren, *Phys. Rev. Lett.* **103**, 257602 (2009).
- [10] Y. Yang, Y. Ji, M. Fang, Z. Zhou, L. Zhang, and X. Ren, *Phys. Rev. Lett.* **123**, 137601 (2019).
- [11] Y. Liu, H. Aziguli, B. Zhang, W. Xu, W. Lu, J. Bernholc, and Q. Wang, *Nature (London)* **562**, 96 (2018).
- [12] V. Ranjan, M. B. Nardelli, and J. Bernholc, *Phys. Rev. Lett.* **108**, 087802 (2012).
- [13] A. J. Lovinger, G. T. Davis, T. Furukawa, and M. G. Broadhurst, *Macromolecules* **15**, 323 (1982).
- [14] K. Tashiro, M. Kobayashi, H. Tadokoro, and E. Fukada, *Macromolecules* **13**, 691 (1979).
- [15] Y. Huang *et al.*, *Nat. Commun.* **12**, 675 (2021).
- [16] F. Yang *et al.*, *Science* **373**, 337 (2021).

- [17] See Supplemental Material at <http://link.aps.org/supplemental/10.1103/PhysRevLett.130.246801> for the experimental methods and demonstration of piezoelectric polymer alloy, the computational procedure of phase-field simulation, the explanation of density functional theory and the structural analysis of piezoelectric polymer alloy.
- [18] K. Omote, H. Ohigashi, and K. Koga, *J. Appl. Phys.* **81**, 2760 (1997).
- [19] T. Furukawa, J. X. Wen, K. Suzuki, Y. Takashina, and M. Date, *J. Appl. Phys.* **56**, 829 (1984).
- [20] F. Oliveira, Y. Leterrier, J. A. Månson, O. Sereda, A. Neels, A. Dommann, and D. Damjanovic, *J. Polym. Sci., Part B* **52**, 496 (2014).
- [21] F. Wang, P. Frubing, W. Wirges, R. Gerhard, and M. Wegener, *IEEE Trans. Dielectr. Electr. Insul.* **17**, 1088 (2010).
- [22] R. S. Pinto, J. P. Serra, J. C. Barbosa, R. Gonçalves, M. M. Silva, S. Lanceros-Méndez, and C. M. Costa, *Macromol. Mater. Eng.* **306**, 2100372 (2021).
- [23] Z. Zhou, D. Qian, and M. Minary-Jolandan, *ACS Biomater. Sci. Eng.* **2**, 929 (2016).
- [24] E. Fukada, *Ultrason. Ferroelectr. Freq. Control.* **47**, 1277 (2000).
- [25] S. B. Liu *et al.*, *Appl. Phys. Lett.* **104**, 172906 (2014).
- [26] K. Tao *et al.*, *Adv. Mater.* **31**, e1807481 (2019).
- [27] T. Zheng, J. Wu, D. Xiao, and J. Zhu, *Prog. Mater. Sci.* **98**, 552 (2018).
- [28] C. T. McKee, J. A. Last, P. Russell, and C. J. Murphy, *Tissue Eng. Part B* **17**, 155 (2011).
- [29] T. Someya, Z. Bao, and G. G. Malliaras, *Nature (London)* **540**, 379 (2016).
- [30] C. Li, C. Guo, V. Fitzpatrick, A. Ibrahim, M. J. Zwierstra, P. Hanna, A. Lechtig, A. Nazarian, S. J. Lin, and D. L. Kaplan, *Nat. Rev. Mater.* **5**, 61 (2019).
- [31] Y. Jiang *et al.*, *Science* **375**, 1411 (2022).
- [32] X. Z. Chen, X. Li, X.-S. Qian, S. Wu, S.-G. Lu, H.-M. Gu, M. Lin, Q.-D. Shen, and Q. M. Zhang, *Polymer* **54**, 2373 (2013).
- [33] Y. Liu, B. Zhang, W. Xu, A. Haibibu, Z. Han, W. Lu, J. Bernholc, and Q. Wang, *Nat. Mater.* **19**, 1169 (2020).
- [34] C. Stadler, S. Hansen, I. Kröger, C. Kumpf, and E. Umbach, *Nat. Phys.* **5**, 153 (2009).
- [35] H. Su, A. Strachan, and W. A. Goddard III, *Phys. Rev. B* **70**, 064101 (2004).